Since January 2020 Elsevier has created a COVID-19 resource centre with free information in English and Mandarin on the novel coronavirus COVID-19. The COVID-19 resource centre is hosted on Elsevier Connect, the company's public news and information website.

Environmental Pollution 289 (2021) 117887

Contents lists available at ScienceDirect

Environmental Pollution

journal homepage: www.elsevier.com/locate/envpol

Characteristics and sources of amine-containing particles in the urban atmosphere of Liaocheng, a seriously polluted city in North China during the COVID-19 outbreak☆

Zheng Li [a], Ruiwen Zhou [a], Yiqiu Wang [b], Gehui Wang [c], Min Chen [a], Yuanyuan Li [a], Yachen Wang [a], Yanan Yi [a], Zhanfang Hou [a], Qingchun Guo [a], Jingjing Meng [a,d,*]

[a] School of Geography and the Environment, Liaocheng University, Liaocheng, 252000, China
[b] Liaocheng Environmental Information and Monitoring Center, Liaocheng, 252000, China
[c] Key Laboratory of Geographic Information Science of the Ministry of Education, School of Geographic Sciences, East China Normal University, Shanghai, 200062, China
[d] State Key Laboratory of Loess and Quaternary Geology, Key Lab of Aerosol Chemistry and Physics, Institute of Earth Environment, Chinese Academy of Sciences, Xi'an, 710075, China

ARTICLE INFO

Keywords:
Amine-containing particles
Diethylamine (DEA)
Gas-to-particle partitioning
Air quality
COVID-19 lockdown

ABSTRACT

The Chinese government issued an unprecedentedly strict lockdown policy to control the spread of the novel coronavirus disease 2019 (COVID-19), significantly mitigating air pollution because of the dramatic reduction of industrial and traffic emissions. To explore the impact of COVID-19 lockdown (LCD) on organic aerosols, the mixing states and evolution processes of amine-containing particles were studied using a single particle aerosol mass spectrometer from January to March 2020 in Liaocheng, which is a seriously polluted city in North China. The counts and percentages of amine-containing particles in total obtained particles during the pre-LCD (547832, 29.8 %) were higher than those during the LCD (283983, 20.7 %) and post-LCD (102026, 18.4 %), mainly due to the reduced emission strength of amines and suppressed gas-to-particle partitioning of amines during the LCD and post-LCD. $^{74}(C_2H_5)_2NH_2^+$ was the most abundant amine marker, which accounted for 98.2 %, 98.4 %, and 96.7 % of all amine-containing particles during the pre-LCD, LCD, and post-LCD, respectively. Correlation analysis and temporal variations indicated that the gas-to-particle partitioning of amines was facilitated by the stronger acidic environment and lower temperature, while the effect of RH and aerosol liquid water content was minor. The A-OC particles were the most abundant type (accounting for ~40 %) throughout the observation period. The temporal profiles and correlation analysis suggested that the impact of the increased O_3 on the amines and their oxidation products (e.g., trimethylamine oxide) was minor. The identified particle types, correlation analysis, and the potential source contribution function results implied that the amine-containing particles were mainly derived from local and surrounding sources during the LCD, while those were mainly affected by long-range transport during the pre-LCD and post-LCD. Our results could deepen the comprehension of the sources and atmospheric processing of amines in the urban area of North China during the COVID-19 outbreak.

1. Introduction

Amines, a group of nitrogen-containing organic compounds, have a significant impact on the global nitrogen cycle, atmospheric chemistry, and wet deposition (Almeida et al., 2013; Ge et al., 2011a). Amines are widely present in rainwater, fog, gas and particle phases (Ge et al., 2011b), and they can be emitted from a variety of natural (e.g., marine environment and vegetation) and anthropogenic (e.g., biomass burning, animal husbandry, vehicle exhaust, and industrial processes) sources (Ge et al., 2011a; Murphy et al., 2007). Laboratory experiments and theoretical calculations have demonstrated that amines are more alkaline than ammonia, although the gaseous concentration of amine is one

☆ This paper has been recommended for acceptance by Dr. Da Chen.

* Corresponding author. School of Geography and the Environment, Liaocheng University, Liaocheng, 252000, China.
E-mail address: mengjingjing@lcu.edu.cn (J. Meng).

https://doi.org/10.1016/j.envpol.2021.117887
Received 27 May 2021; Received in revised form 9 July 2021; Accepted 30 July 2021
Available online 31 July 2021

or two orders of magnitude lower than ammonia (Cheng et al., 2018; Ge et al., 2011a; Sorooshian et al., 2008). The concentration of amines is only 14%–23 % of ammonium, but it has been thought to be a key basic compound even in aerosol particles containing ammonium (Sorooshian et al., 2008). Amines can react directly with organic and inorganic acids such as sulfuric acid, nitric acid, and acetic acid to form particulate salts because of the strong alkalinity and high water solubility, thereby playing an important role in enhancing the atmospheric nucleation (Zhang et al., 2012). Furthermore, amines can react with oxidants such as O_3, OH, and NO_3 radicals to form semi-volatile and non-volatile chemical species, which can significantly contribute to the formation of secondary organic aerosol (SOA) (Lee and Wexler, 2013; Murphy et al., 2007). Therefore, amine particles play an important role in the new particle formation (Creamean et al., 2011; Huang et al., 2012; Kurten et al., 2016).

The mass concentrations and temporal distributions of amines in Chinese megacities (e.g., Guangzhou, Nanjing and Shanghai) have been studied extensively based on the traditional filter sampling methods (Cheng et al., 2020; Liu et al., 2018; Shen et al., 2017). However, the traditional off-line sampling is time consuming and the samples may be reacted with each other during the sampling process. In recent years, single particle aerosol mass spectrometer (SPAMS) and aerosol time-of-flight mass spectrometry (ATOFMS) have been widely employed to study the chemical compositions, mixing states, and formation processes of amine-containing particles at a high time resolution (Chen et al., 2019; Cheng et al., 2018; Healy et al., 2015; Lian et al., 2020b; Qin et al., 2012). The gas-to-particle partitioning of amine is influenced by many factors, such as aerosol liquid water content (ALWC), particulate acidity, and atmospheric oxidation capacity, as well as meteorological conditions including relative humidity (RH) and temperature (Chen et al., 2019; Cheng et al., 2018). Previous studies in southern China found that high RH condition was favorable for the enhancement of amine-containing particles (Chen et al., 2019; Cheng et al., 2018; Zhang et al., 2012). Huang et al. (2012) reported the higher counts of amine-containing particles during winter than that during summer, due to the lower temperature and higher RH conditions during winter. Rehbein et al. (2011) also found that cloud/fog events could enhance the gas-to-particle partitioning of trimethylamine (TMA), which was highly dependent on the aerosol water content. Zhang et al. (2012) proposed that the enhanced TMA in the urban atmosphere of Guangzhou in southern China was mainly attributed to the acid-base chemistry and gas-to-particle partitioning. In addition, the strong particle acidity could promote the gas-to-particle partitioning of diethylamine (DEA) (Ge et al., 2011b). Both laboratory and field studies have indicated that alkylamines are able to replace NH_4^+ to form ammonium-sulfuric acid clusters and ammonium nitrate nanoparticles (Bzdek et al., 2010; Cheng et al., 2018; Lloyd et al., 2009; Sauerwein and Chan, 2017). Also, the gaseous amines were found to be effective precursors of the new atmospheric particles by enhancing the ternary nucleation of H_2SO_4-H_2O clusters (Kirkby et al., 2011; Yao et al., 2018). Therefore, it is essential to understand the temporal variations, sources, and evolution processes of amine as well as the influencing factors of gas-to-particle partitioning.

A novel coronavirus disease (COVID-19) abruptly broke out at the end of 2019 and it has caused a huge socioeconomic disruption all over the world (Chang et al., 2020). There have been more than 184.8 million cases of infection confirmed, including about 4.0 million deaths by July 9, 2021 (https://covid19.who.int/). To curb the spread of this pandemic, the Chinese government implemented a preventive lockdown (LCD) beginning at the end of January 2020 (Li et al., 2020a; Lian et al., 2020a). During the LCD, the emissions of anthropogenic pollutants dropped dramatically (Liu et al., 2021; Yuan et al., 2021). For example, five air pollutants including $PM_{2.5}$, PM_{10}, CO, NO_2, and SO_2 from 44 cities in northern China during the LCD decreased by 4.6%–24.7 % than those during the pre-LCD, largely attributed to the implementation of traffic restrictions during the pandemic (Bao and Zhang, 2020). Unexpectedly, several serious haze events occurred simultaneously in northern China (Huang et al., 2021; Le et al., 2020). Field measurements, model simulations, and satellite observations have demonstrated that the occurrence of haze pollution during the LCD was mainly launched by the adverse meteorological conditions, the increased formation of the secondary aerosols initiated by the high concentration of O_3, along with the ongoing emissions from petrochemical facilities and power plants (Huang et al., 2021; Li et al., 2020a; Meng et al., 2021; Wang et al., 2020). In addition, the enhanced heterogeneous chemistry associated with the high RH and ALWC was also regarded as an important contributor to haze episodes (Le et al., 2020; Meng et al., 2021). There have been several studies focused on the impact of the LCD on the atmospheric pollution and haze formation, but the effect of the LCD on the chemical compositions, mixing states, and the formation processes of the organic aerosols (OAs) from ground observations in the urban atmosphere is not well known. During the LCD, the dramatically reduction of anthropogenic emissions (e.g., NO_x, VOCs) lead to the increased concentration of O_3, which further resulted in the OAs being more oxidized (Liu et al., 2021; Meng et al., 2021). However, there still has been little information about the aging process of OAs, especially amines. In this work, SPAMS was used to investigate the mixing states and formation processes of amine-containing particles in the pre-LCD, LCD and post-LCD to explore the effect of the LCD policies on the evolution processes of amines-containing particles in the urban areas of NCP. This investigation is helpful for us to understand the atmospheric chemical composition and mechanism of amines, which in turn will provide insights into important formation and mitigation of haze events in the NCP.

2. Methods

2.1. Aerosol sampling

Liaocheng, as one of the "2 + 26" air pollution transmission channel cities in the Beijing-Tianjin-Hebei region, is located in the southwest of Shandong Province in the NCP, where severe air pollution usually occurs. Field observations were carried out at a national air quality monitoring station (36.44 °N, 116.02 °E) at Liaocheng University, which is located in the southeast of the city of Liaocheng. The SPAMS was set on the rooftop of a six-story building, which is approximately 25 m above the ground. The supersite is surrounded by residential communities and main roads without significant industrial sources nearby. The ambient single particle was collected by SPAMS (0515-R Model, Hexin Analytical Instrument Co., Ltd., China) at a 1-h resolution. Five air pollutants including $PM_{2.5}$, SO_2, NO_2, CO, and O_3, and meteorological parameters were obtained from the website of the Environmental Protection Bureau of Liaocheng (http://www.lchbj.gov.cn).

To eliminate the spread of the virus among humans, Wuhan city in China was firstly locked down on 23 January 2020. The Shandong provincial government issued the first-level emergency response for epidemic prevention and control on 24 January 2020, thus we defined the pre-LCD stage from 9 to 23 January 2020. The burning of fireworks and firecrackers displayed as a traditional way to celebrate Chinese lunar New Year from 25 to 30 January 2020, which can cause severe haze events. To avoid the effect of fireworks and firecrackers burning on amine-containing particles, we defined the LCD stage from 1 to 15 February 2020. In late February of 2020, the COVID-19 cases began to decrease and the factories and public spaces started to reopen in Shandong Province, thus we defined post-LCD stage from 1 to 15 March 2020. Therefore, the whole sampling period was divided into three stages: pre-LCD (from 9 to 23 January 2020), LCD (from 1 to 15 February 2020), and post-LCD (from 1 to 15 March 2020).

2.2. Data analysis

The detailed description of SPAMS is available in previous literatures (Li et al., 2011; Li et al., 2020b). Briefly, ambient aerosols were sampled

through a 100 μm metal orifice into instrument at a flow rate of 75 mL min^{-1}. Particles pass consecutively through two pre-positioned laser beams (Nd:YAG, 532 nm), and the aerodynamic diameter of each particles is determined via its time of flight. Then, the particles were desorption/ionization using 266 nm Nd:YAG pulsed laser beams. After ionization, the positive and negative ions are detected using a Z-shaped bipolar time-of-flight mass spectrometer. The SPAMS data were analyzed using the COCO V3.0 toolkit in Matlab 2014b (Math Work Inc., Natick, MA, USA). According to previous studies (Chen et al., 2019; Cheng et al., 2018; Huang et al., 2012; Lian et al., 2020b; Qin et al., 2012; Zhang et al., 2012), amine-containing particles were identified by querying m/z $^{59}(CH_3)_3N^+$ (TMA), $^{74}(C_2H_5)_2NH_2^+$ (DEA), $^{86}[(C_2H_5)_2NCH_2^+$ or $C_3H_7NHC_2H_4^+]$ (DEA, DPA or TEA, defined as TEA in this study) (Angelino et al., 2001), $^{101}(C_2H_5)_3N^+$ (TEA), $^{102}(C_3H_7)_2NH_2^+$ (DPA), and $^{143}(C_3H_7)_3N^+$ (TPA) (Table S1). In this study, amine-containing particles were identified if the relative peak area of the marker ions listed above is higher than 1 %. It has been reported that the m/z of +46 could be defined as $^{46}(CH_3)_2NH_2^+$ or $^{46}Na_2^+$ (Cheng et al., 2018). As shown in Fig. S1, the m/z +46 containing particles had no other amine markers as listed above. These particles were enriched with $^{62}Na_2O^+$ and $^{81}Na_2Cl^+$ (Fig. S1), indicating that the m/z +46 particles were more likely sodium salts. In addition, the numbers of particles containing the m/z +46 were much lower than other amines (≤1 % in total detected particles). Therefore, the particles containing m/z +46 were not defined as amine-containing particles in this study.

2.3. Aerosol liquid water content (ALWC)

Water-soluble inorganic ions were also measured per hour using an online ion chromatograph (IC, WARGA, Hangzhou Juguang Analytical Company, China) coupled with a $PM_{2.5}$ sampling inlet during the entire sampling period. The calculation of ALWC in $PM_{2.5}$ samples was calculated using the ISORROPIA-II model, which treated the Na^+ - NH_4^+ - K^+ - Ca^{2+} - Mg^{2+} - SO_4^{2-} - NO_3^- - Cl^- system (Wu et al., 2018). The forward mode with a metastable state in the ISORROPIA model was chosen in this study.

2.4. Potential source contribution function

The 72 h air mass back-trajectories (500 m above the ground, 1h resolution) were simulated using the Hybrid Single-particle Lagrangian Integrated Trajectory (HYSPLIT) model (Cheng et al., 2020), based on the meteorological data downloaded from the National Oceanic and Atmospheric Administration (NOAA) Global Data Assimilation System (GDAS, spatial resolution 1 ° × 1 °). The Potential Source Contribution Function (PSCF) method was applied to identify the potential source regions and the individual contributions of three mainly amine-containing particles by using the TrajStat plugins on MeteoInfoMap software (Wang et al., 2009). The study region was divided into $i \times j$ grid cells (ij) and the value of PSCF is defined as:

$$PSCFij = \frac{mij}{nij} \quad (1)$$

where n_{ij} is the number of endpoints through the ij grid cell, and m_{ij} is the total number of trajectory endpoints concentrated in the same cell that exceeded the criterion value (the 75th percentile). To decrease the effect of small values of n_{ij}, the PSCF values were multiplied by an arbitrary weight function W_{ij} (Wang et al., 2009), which was defined as follows:

$$Wij = \begin{cases} 1.00, & 3n_{mean} < nij \\ 0.70, & n_{mean} < nij < 3n_{mean} \\ 0.42, & 0.5n_{mean} < nij < n_{mean} \\ 0.05, & nij < 0.5n_{mean} \end{cases} \quad (2)$$

3. Results and discussion

3.1. Overview of the campaign during the COVID-19 pandemic

Temporal variations in the concentration of $PM_{2.5}$ and gaseous pollutants during the whole sampling campaign are shown in Fig. 1 along with the meteorological parameters. $PM_{2.5}$ concentration in the whole observation period showed a continuous decreasing trend with averages of 136.0 ± 46.9, 70.3 ± 37.5, and 53.5 ± 29.4 μg m^{-3} during the pre-LCD, LCD, and post-LCD, respectively (Table 1), indicating that the air quality was significantly improved because of the substantial reduction of pollutant emissions during the COVID-19 control period (Li et al., 2020b). The mean concentration of $PM_{2.5}$ (96.6 ± 52.5 μg m^{-3}) was significantly higher than that during the same period in other Chinese urban regions such as Beijing (53.9 μg m^{-3}) (Sun et al., 2020), Lanzhou (45.6 ± 14.9 μg m^{-3}) (Xu et al., 2020a) and Shanghai (35.5 ± 26.2 μg m^{-3}) (Jia et al., 2020), suggesting that Liaocheng was still facing the severe air pollution. Previous studies have shown that the relatively high $PM_{2.5}$ concentration during the COVID-19 lockdown in the NCP was largely driven by both the stagnant meteorological conditions and enhanced secondary aerosol formation (Huang et al., 2021; Le et al., 2020; Wang et al., 2020).

Compared with the pre-LCD period, the average concentration of SO_2 and NO_2 reduced by 36.4 % and 70.4 % during the LCD, but increased significantly to 9.7 ± 9.1, 35.6 ± 19.9 μg m^{-3} (Table 1), due to the recovery of industrial production during the post-LCD (Li et al., 2020a; Pei et al., 2020). As an important tracer of primary combustion emissions (Zhang et al., 2021), CO presented a decreasing trend similar to that of $PM_{2.5}$ concentration throughout the LCD (Fig. 1). It is a clear fact that the decrease of NO_2 was the most conspicuous during the LCD because of the sharp drop of industrial exhausts and vehicular traffic (Li et al., 2020a; Pei et al., 2020). However, the changes of SO_2 among three observation periods was the least, which was attributed to the uninterrupted emissions of SO_2 from power plants and petrochemical facilities (Le et al., 2020). O_3 can be used as an indicator of atmospheric oxidation capacity, because it mainly originated from the photochemical reaction of NO_x and volatile organic compounds (VOCs) (Li et al., 2020b; Meng et al., 2021). In contrast to other four air quality pollutant parameters, O_3 concentration exhibited a similar level during LCD and post-LCD (62.4 ± 23.9 μg m^{-3} versus 59.2 ± 32.9 μg m^{-3}; Table 1 and Fig. 1), but increased by approximately two times compared to that during the pre-LCD (31.2 ± 23.9 μg m^{-3}), indicating that the atmospheric oxidation capacity was dramatically improved during the LCD and post-LCD. The opposite variation of O_3 with other air pollutants was also reported in other Chinese megacities during the LCD (Tobías et al., 2020; Zheng et al., 2020). The formation of O_3 is principally originated form the NO_x-saturated regime in the urban atmosphere of China due to the shortage of HO_x radicals during winter (Meng et al., 2021). The depletion of NO_2 during the LCD and the post-LCD could result in the sharp reduction of NO, and further contributed to the urban O_3 bumping up (Monks et al., 2015). On the other hand, the sink of nitrogen oxide (NO) alleviated the consumption of O_3 (titration, $NO + O_3 = NO_2 + O_2$), leading to an increase in O_3 during the LCD and the post-LCD (Xu et al., 2020b; Zheng et al., 2020). Moreover, the higher temperature and stronger solar radiation conditions during the LCD and the post-LCD could promote the production of O_3 (Meng et al., 2021).

Secondary inorganic aerosols (SIA, sum of concentrations of SO_4^{2-}, NO_3^-, and NH_4^+) were the dominant species of $PM_{2.5}$, which showed a decreasing trend in pace with the change of $M_{2.5}$ and CO concentrations throughout the campaign (Fig. 1). The concentrations of NH_4^+, SO_4^{2-}, and NO_3^- during the pre-LCD were 23.3 ± 7.9, 24.8 ± 10.5, and 33.3 ± 12.8 μg m^{-3}, respectively. Their concentration decreased to 11.5 ± 6.8, 10.6 ± 6.2, and 12.2 ± 5.0 μg m^{-3} during the LCD and to 11.3 ± 9.3, 5.7 ± 2.9, and 9.4 ± 8.7 μg m^{-3} during the post-LCD (Table 1). The mass ratio of NO_3^- to SO_4^{2-} can be used as an indicator of the relative importance of vehicle exhaust versus the stationary sources of nitrogen

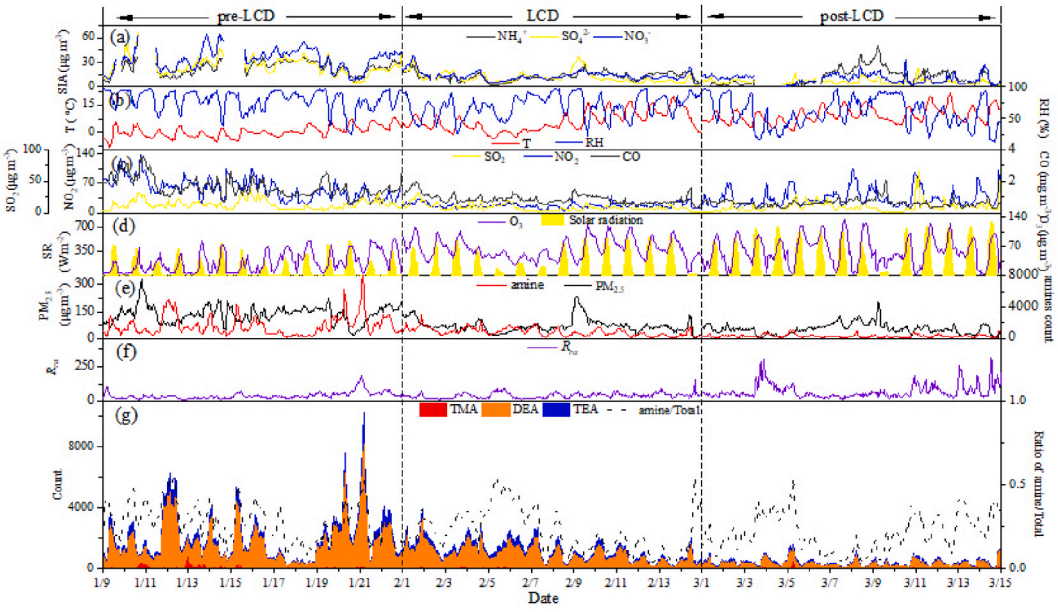

Fig. 1. Temporal variations of meteorological parameters, R_{ra} and the concentrations of $PM_{2.5}$ and gaseous pollutants, as well as major amine-containing particles during the whole sampling period.

Table 1
Differences in meteorological factors, gaseous species, secondary inorganic species, $PM_{2.5}$ concentration, and the counts of major amine-containing particle during the pre-LCD, LCD, and post-LCD in Liaocheng.

	Pre-LCD	LCD	Post-LCD
Meteorological parameters			
T (°C)	0.4 ± 3.1	5.7 ± 4.9	9.3 ± 4.1
RH (%)	80.0 ± 15.6	70.0 ± 17.6	59.0 ± 23.1
Wind speed (m s^{-1})	1.0 ± 0.5	1.6 ± 0.8	1.8 ± 1.0
Solar radiation (W m^{-2})	166 ± 135	210 ± 181	302 ± 232
Gaseous pollutants			
SO_2 (μg m^{-3})	13.2 ± 7.0	8.4 ± 5.3	9.7 ± 9.1
NO_2 (μg m^{-3})	58.1 ± 23.9	17.2 ± 5.7	35.6 ± 19.9
CO (mg m^{-3})	1.6 ± 0.6	0.9 ± 0.3	0.6 ± 0.2
O_3 (μg m^{-3})	31.2 ± 23.9	62.4 ± 23.9	59.2 ± 32.9
Number fraction of major amine (%)			
TMA	0.9 ± 2.8	0.4 ± 1.2	0.7 ± 3.4
DEA	29.3 ± 44.0	20.3 ± 32.8	17.8 ± 22.8
TEA	6.4 ± 10.8	5.4 ± 8.5	4.9 ± 6.4
Amine/total particles ratio	29.8 ± 10.7	20.7 ± 10.0	18.4 ± 9.8
Secondary inorganic species (μg m^{-3})			
NH_4^+	23.3 ± 7.9	11.5 ± 6.8	11.3 ± 9.3
SO_4^{2-}	24.8 ± 10.5	10.6 ± 6.2	5.7 ± 2.9
NO_3^-	33.3 ± 12.8	12.2 ± 5.0	9.4 ± 8.7
Others			
$PM_{2.5}$ (μg m^{-3})	136 ± 46.9	70.3 ± 37.5	53.5 ± 29.4
R_{ra}	38.8 ± 21.5	33.6 ± 16.1	80.0 ± 71.8
ALWC (μg m^{-3})	202 ± 193	63.4 ± 113	28.1 ± 39.0
$NH_4^+/PM_{2.5}$	17.1 ± 6.2	16.4 ± 7.7	21.1 ± 11.8
NO_3^-/SO_4^{2-}	1.4 ± 0.3	1.2 ± 0.4	1.7 ± 0.9

and sulfur in the aerosol (Dai et al., 2018; Xu et al., 2019). The lower ratio of NO_3^-/SO_4^{2-} suggested that the contribution of stationary sources was more important than the mobile sources (Xu et al., 2019). The average ratio (1.2 ± 0.4) of NO_3^-/SO_4^{2-} during the LCD was lower than that during the pre-LCD (1.4 ± 0.3) and post-LCD (1.7 ± 0.9), indicating the more predominant contribution of stationary sources than the mobile sources due to the substantial drop in on-road vehicular traffic during the LCD. As shown in Table 1 and Fig. 1, temperature, solar radiation, and wind speed presented a continuous increasing trend throughout the LCD. Conversely, RH displayed a continuous descending trend, with average values of 80.0 ± 15.6, 70.0 ± 17.6, and 59.0 ± 23.1% during the pre-LCD, LCD, and post-LCD, respectively.

3.2. Characteristics of amine-containing particles

The counts and fractions of amine-containing particles in the whole observation period were summarized in Table S1. A total of 547832, 283983 and 102026 amine-containing particles were detected during the pre-LCD, LCD, and post-LCD, which accounted for 29.8 %, 20.7 %, and 18.4 % of the total detected particles, respectively. The higher counts and fractions of amine-containing particles during the pre-LCD were largely explained by the preferred gas-to-particle partitioning of gaseous amines under the lower temperature and higher RH conditions during the pre-LCD (Fig. 1). The average fraction (22.0 %) of amine-containing particles in Liaocheng was higher than that reported in urban background site in Switzerland (16.5 %) and some megacities in China such as Chongqing (12.7 %) and Guangzhou (0.8 %) (Chen et al., 2019; Healy et al., 2015; Lian et al., 2020b). In addition, Healy et al. (2015) reported that the higher concentration of amines in the rural site than that in the urban and industrial sites was primarily due to the enhanced anthropogenic emissions of amines from agriculture activity and animal husbandry. The relatively high fraction of amines in this study might be associated with strong emission sources and favorable meteorological conditions in Liaocheng (detailed discussions will be described in sections 3.3 and 3.4). Similar to the distributions of amine-containing particles at a rural site in the Pearl River Delta of China (Cheng et al., 2018), the most abundant amine marker was $^{74}(C_2H_5)_2NH_2^+$, accounting for 98.2 %, 98.4 % and 96.7 % of all amine-containing particles during the pre-LCD, LCD, and post-LCD, respectively, followed by $^{86}[(C_2H_5)_2NCH_2^+$ or $C_3H_7NHC_2H_4^+]$, and $^{59}(CH_3)_3N^+$. The total fractions of ^{101}TEA-, ^{102}DPA-, and ^{143}TPA--containing particles were negligible, which was less than 0.5 % of all detected amine-containing particles throughout the observation period.

As shown in Fig. S2, the positive mass spectra of amine-containing particles were characterized by the strong intensities of carbonaceous fragments such as $C_nH_m^+$ and C_n^+ (n = 1–5, m = 1–3) in addition to the amine marker ions of $^{74}C_4H_{12}N^+$ and $^{86}C_5H_{12}N^+$, while the negative mass spectra were dominated by the high abundances of secondary species including $^{46}NO_2^-$, $^{62}NO_3^-$ and $^{97}HSO_4^-$, and carbon-nitrogen fragments ($^{26}CN^-$ and $^{42}CNO^-$) during the whole sampling campaign. As an important tracer for biomass burning (Bi et al., 2011), levoglucosan markers (m/z $^{45}CHO_2^-$ and $^{59}C_2H_3O_2^-$) and $^{115}K_2Cl^+$ were also observed in the negative mass spectrum, indicating that biomass

burning was a major source of amines. In addition, oxidized organic species such as $m/z^{89}C_2HO_3^-$ and $^{43}C_2H_3O^+$ were also observed during the whole campaign, indicating that the particles had experienced substantial aging processes. As shown in Fig. S2, the signal intensity of $m/z^{40}Ca^+$ was observed to be stronger during the LCD and post-LCD than that during the pre-LCD. Moreover, the determination coefficient (R^2) between amine-containing particles and Ca^+-containing particles was higher during the LCD (0.47, $P < 0.01$) and post-LCD (0.58, $P < 0.01$) than that during the pre-LCD (0.11, $P > 0.05$), which indicated the vitally significant impact of dust source on the amine-containing particles during the LCD and post-LCD. The enhanced impact of dust source on the amine-containing particles can be attributed the increased wind speed during the LCD and post-LCD (Table 1). To evaluate the acidic environment of amine-containing particles, the relative aerosol acidity (R_{ra}) was defined as the ratio of total peak areas of nitrate ($m/z^{62}NO_3^-$) and sulfate ($m/z^{97}HSO_4^-$) to the peak area of ammonium ($m/z^{18}NH_4^+$) (Denkenberger et al., 2007). Our previous study has obtained a significant correlation ($R^2 = 0.62$, $P < 0.01$) between the in situ particle pH (pH_{is}) calculated from inorganic ions using the ISORROPIA-II model and relative acidity ratio estimated by the SPAMS, confirming the validity of using R_{ra} for evaluating particle acidity (Meng et al., 2021). As shown in Fig. 1(f), the average value of R_{ra} (71.3 ± 51.3) during the post-LCD was approximately twice higher than that during the pre-LCD (41.3 ± 24.6) and the LCD (40.9 ± 18.1), suggesting the more acidic nature of amine-containing particles during the post-LCD.

The different peak modes of size distribution suggested the differences in the atmospheric evolution process and sources of amine particles (Liu et al., 2017). The unscaled size distributions of the DEA-, TEA-, and TMA-containing particles were shown in Fig. S3. The amines-containing particles mainly existed in the droplet mode from 0.3 to 1.4 μm in the whole sampling period, possibly attributed to the gaseous amine condensation on and/or reaction with fine mode particles (Cheng et al., 2018). The amine-containing particles during the pre-LCD and post-LCD showed unimodal distributions and peaked at ~0.48 and ~0.54 μm, respectively. However, the unscaled size distributions of amine-containing particles during the LCD exhibited a bimodal distribution with a larger peak at ~0.48 μm and a smaller peak at ~0.66 μm. The broad size peak and distribution range of amine-containing particles during the LCD and post-LCD were possibly resulted from more complex sources and/or gaseous amine condensation or reaction with the coarser particles during long-distance transport. The DEA- and TEA-containing particles showed a similar pattern of variation as the total amine-containing particles in the three sampling periods (Fig. S3).

3.3. Gas-to-particle partitioning of amine-containing particles

The partitioning of gaseous amines to the particle phase is mainly through both acid-base reactions and direct dissolution (Liu et al., 2018). Under relatively lower RH conditions, reacting with the acidic species (e.g., HNO_3 (g) and H_2SO_4 (g)) may be the dominant way for the gaseous amines condensed into the particle phase (Ge et al., 2011a, b). However, the partitioning of amines from the gaseous phase to the particle phase is mainly via direct dissolution under relatively high RH conditions (Liu et al., 2018). Several field observations have demonstrated that the high RH condition is favorable for the gas-to-particle partitioning of amines (Chen et al., 2019; Zhang et al., 2012). The DEA-containing particles were the most abundant amine-containing particles in the whole sampling period. Therefore, we took the DEA-containing particles as an example to investigate the effect of RH on gas-to-particle partitioning of amines. Box plots of relative peak area (RPA) of DEA under different RH were shown in Fig. 2(a). When RH increased from the range of lower than 45 % to the range of 85 %–100 %, the median RPA of the DEA containing particles increased from 3.4 % to 3.8 %, from 3.2 % to 3.5 %, and from 3.5 % to 3.8 % during the pre-LCD, LCD, and post-LCD, respectively. Such a small rise (0.3–0.5 %) in RPA of DEA under different RH indicated a minor impact of RH on the gas-to-particle partitioning of amine-containing particles. High water content could enhance the acid-base reaction by dissolving ammonium salts into their ionic forms and shifting the gas-to-particle equilibrium of amines to the particle phase because of the high aqueous solubility of amines (Huang et al., 2012; Rehbein et al., 2011). ALWC is controlled by both SIA concentrations and RH (Yi et al., 2021). Both SIA concentrations and RH during the pre-LCD were higher than those during the LCD and post-LCD, leading to the ALWC during the pre-LCD (201.9 ± 193.6 μg m^{-3}) being 3.2 times and 7.2 times higher than that during (63.7 ± 113.4 μg m^{-3}) and post- (28.1 ± 39.0 μg m^{-3}) the LCD, respectively. As shown in Fig. 3(b–d), the number of amines and amine/total ratio did not exhibit similar trends with RH and ALWC, suggesting that the effects of RH and ALWC on amine-containing particles were negligible. Therefore, the more abundant particle amines during the pre-LCD may be influenced by particle acidity, temperature, and source strength of amines. It is noteworthy that the median RPA of the DEA containing particles was the highest during the post-LCD, followed by during the pre-LCD and during the LCD when RH was lower than 65 % (Fig. 3(a)), which was in accordance with the distribution of R_{ra} in section 3.2. The strong acidic conditions can facilitate the partitioning of gaseous DEA into the aqueous phase by the formation of aminium salts through reacting with acids of HCl, HNO_3 and H_2SO_4 (Chen et al., 2019). These results implied that the aerosol acidity was a key factor influencing the

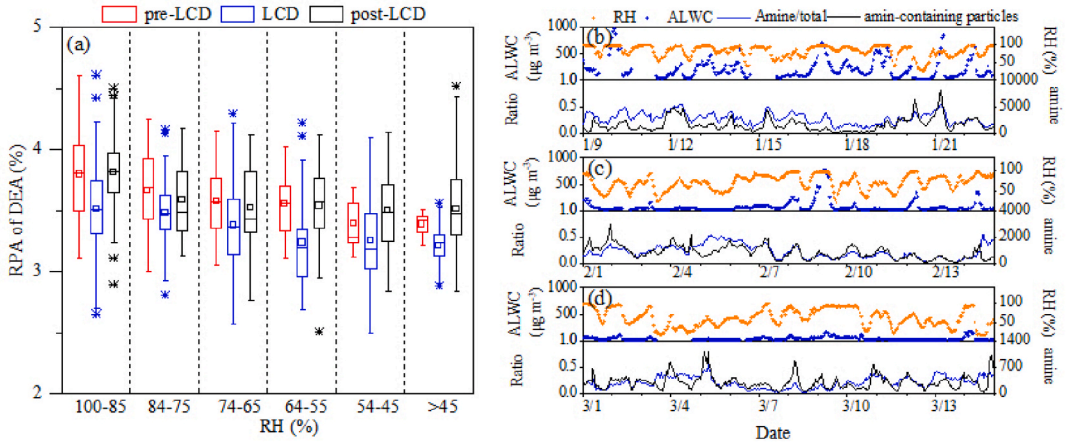

Fig. 2. (**a**) Box plots of the hourly relative peak area (RPA) of DEA under different RH conditions during the pre-LCD, LCD, and post-LCD; Temporal variations of RH, aerosol liquid water content (ALWC), number of amine-containing particles and the number fraction of amine/total detected particles during the (**b**) pre-LCD, (**c**) LCD and, (**d**) post-LCD.

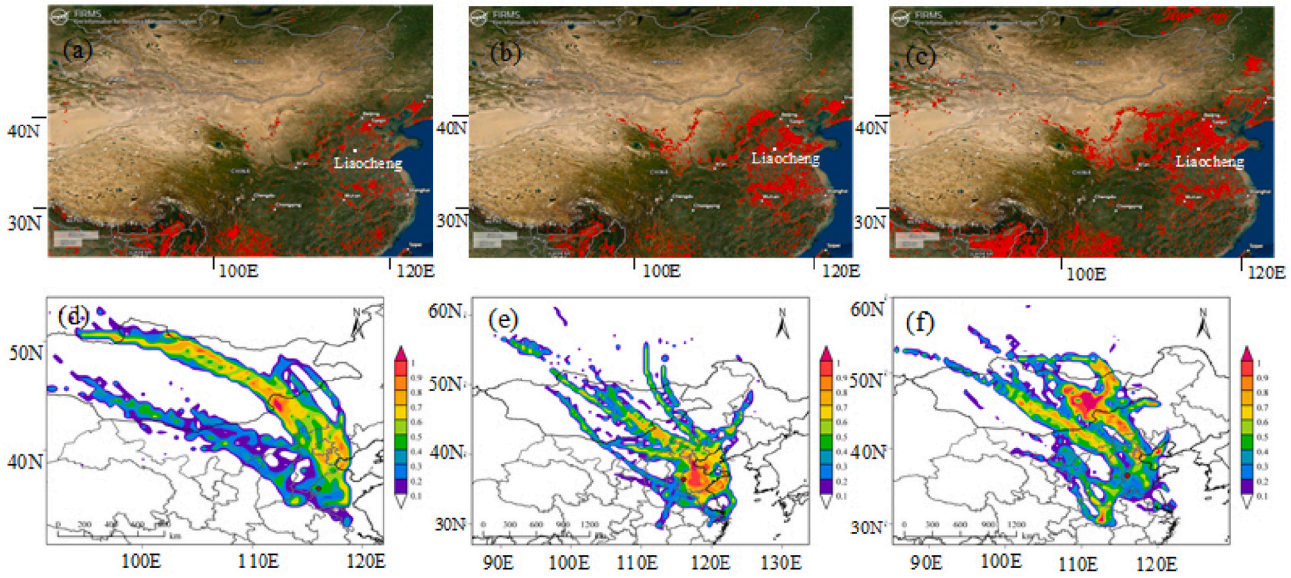

Fig. 3. Fire spots provided by Fire Information for Resource Management System, (FIRMS) (https://firms.modaps.eosdis.nasa.gov) during the (**a**) pre-LCD, (**b**) LCD, and (**c**) post-LCD; and the results of WPSCF analysis of total amine-containing particles during the (**d**) pre-LCD, (**e**) LCD, and (**f**) post-LCD.

gas-to-particle partitioning of amines when RH was lower than 65 %. Moreover, the ratio of amine/total detected particles correlated well ($R^2 > 0.30$, $P < 0.01$) with R_{ra} during the pre-LCD, LCD and post-LCD, respectively, again suggesting that the enhancement of aerosol acidity could promote the partitioning of amines from the gaseous phase to the particle phase.

Lower temperature can facilitate gaseous amines to enter the particle phase via gas–particle partitioning (Huang et al., 2012). The fractions of amine-containing particles showed a negative correlation with temperature during the whole sampling period ($R^2 = 0.32$, $P < 0.01$), indicating that the lower temperature can promote the distribution of amines to particle phase. The weaker correlations during the pre-LCD and post-LCD indicated that temperature was less important than other factors such as RH and R_{ra} in these two observation periods. The mixing state of amine-containing particles with sulfate, nitrate and ammonium were shown in Table S2. More than 96 % of amines were found mixing with sulfate and nitrate in the whole sampling period. The extremely high abundances of sulfate and nitrate in particulate amines indicated the possible production of aminium sulfate and nitrate salts. The abundance of ammonium in amine-containing particles was lower than sulfate and nitrate, which was in line with the smaller number of ammonium-containing particles in all detected particles (Table S2). In addition, the peak areas of DEA well correlated with sulfate ($R^2 > 0.62$, $P < 0.01$) and nitrate ($R^2 > 0.63$, $P < 0.01$) during the pre-LCD, LCD, and post-LCD, respectively, confirming that particulate amines principally existed in the forms of aminium sulfate and aminium nitrate (Ge et al., 2011a). The contribution of NH_4^+ to $PM_{2.5}$ was much higher during the post-LCD (21.1 ± 11.8 %) than that during the pre-LCD (17.1 ± 6.2 %) and LCD (16.4 ± 7.7 %). The lower number of amine-containing particles and the ratio of amines to the total detected particles during the post-LCD was mainly because the gas-to-particle partitioning of amines might be restrained under a relatively rich NH_4^+ state during the post-LCD.

In addition, no significant correlations ($R^2 < 0.38$, $P < 0.01$) were obtained between O_3 and amine-containing particles during three observation periods, indicating the effect of O_3 on the formation of amine-containing particles was minor. As the oxidation product of TMA, trimethylamine oxide (TMAO) ($m/z = 76$) was identified in this study to further investigate the effect of O_3 on the amine-containing particles. The counts of the TMAO-containing particles were obtained to be 42155, 46476, and 20207, and the fractions of TMAO in the total detected particles were 2.5 %, 9.1 %, and 4.9 % during the pre-LCD, LCD, and post-LCD, respectively. There was no significant correlation ($R^2 < 0.3$, $P < 0.01$) between TMAO particles (or the ratio of TMAO/TMA) and O_3 in these three observation periods (Fig. S4). However, the temporal profiles of TMAO and TMAO/TMA ratio exhibited similar diurnal variations with RH and ALWC during the whole observation period (Fig. S5). These results demonstrated that the probable formation of TMAO was closely associated with the aqueous oxidization reaction at night, rather than the O_3-dominated photochemical oxidation, thus the number count and fraction of TMAO showed higher values in nighttime (139.9 ± 48.2; 14.0 ± 8.1 %) than in daytime (74.1 ± 51.5; 10.5 ± 9.9 %) in the whole observation period. It has been reported that the aqueous oxidation launched by NO_3 radicals in nighttime significantly contributed to the production of TMAO, but the contribution of photochemical oxidation of amines with O_3 was negligible (Lian et al., 2020b; Tang et al., 2013). Therefore, the increased concentration of O_3 during the LCD and post-LCD was not a vital influencing factor determining the enhanced TMAO.

3.4. Potential source contribution function

As shown in Fig. S6, the amine-containing particles were classified into six types, including amine-organic carbon (A-OC), amine-elemental carbon (A-EC), A-EC and OC combined particles (A-OCEC), A-OCEC aged, sea salt, and biomass burning (BB), which accounted for 95 % of all amine-containing particles. The A-OC particles were the most abundant type, contributing to approximately 40.0 % of the total amine particles in the whole sampling period (Fig. S7). There were no significant correlations between A-OC types with SO_2 and NO_2 ($R^2 < 0.4$, $P < 0.01$), respectively, indicating that the impact of fossil fuel combustion on A-OC particle type was negligible. The positive mass spectrum of A-OC was characterized by the strong signals of amines (m/z $^{74}(C_2H_5)_2NH_2^+$ and $^{86}[(C_2H_5)_2NCH_2^+$ or $C_3H_7NHC_2H_4^+]$), and hydrocarbon fragments (m/z $^{27}C_2H_3^+$, $^{37}C_3H^+$, $^{51}C_4H_3^+$, and $^{63}C_5H_3^+$), while the negative mass spectrum was dominated by nitrate and sulfate (m/z $^{46}NO_2^-$, $^{62}NO_3^-$, and $^{97}HSO_4^-$). The A-OCEC particles was characterized by strong signals of hydrocarbon fragments, EC fragments (m/z $^{36}C_3^{+/-}$, $^{48}C_4^{+/-}$ and $^{60}C_5^{+/-}$) and amines fragments in the mass spectra, and with minor peaks of nitrate and sulfate (m/z $^{46}NO_2^-$, $^{62}NO_3^-$, and $^{97}HSO_4^-$) in the negative mass spectra. The A-OCEC particles were relatively stable and accounted for 21.1%–24.1 % of amine-

containing particles in these three sampling periods. The A-OCEC aged particles had a similar chemical composition to A-OCEC, but with stronger relative intensities of secondary species including sulfate, nitrate, and ammonium. The A-OCEC aged type exhibited the higher fraction during the LCD (21.7 %) than that during the pre-LCD (19.4 %) and post-LCD (15.0 %), indicating that the atmosphere was more aged during the LCD due to the higher concentration of O_3. The higher (7.8 %) fraction of sea salt type was obtained during the LCD compared to that in the pre-LCD (4.8 %) and post-LCD (5.2 %) periods, implying the increased contribution of sea salt to particles during LCD. A-EC particles were characterized by a serious of elemental carbon fragments in both the positive and negative mass spectra. Previous study demonstrated that EC in amine-containing particles were mostly derived from fresh mobile emissions (Huang et al., 2012). The fraction of A-EC particle during the LCD (1.1 %) was about 2.5 times lower than that during the pre-LCD (3.8 %) and post-LCD (3.7 %), which may be attributed to the sharp reduction of on-road vehicle numbers because of the lockdown measurement. As shown in Fig. S7, the fraction of BB particle type showed an increasing trend from 4.2 % during the pre-LCD to 7.0 % during the LCD to 12.1 % during the post-LCD. Similarly, the gradual increase of the number of fire spots from the pre-LCD to the LCD was also observed according to the National Aeronautics and Space Administration (NASA) satellite observation (Fig. 3), suggesting that the increased BB in Liaocheng and surrounding regions during the post-LCD significantly contributed to the formation of amine particles in the urban areas of NCP.

The potential source regions for amine-containing particles during three sampling periods are shown in Fig. 3(d–f). During the pre-LCD, the WPSCF values for amine-containing particles (Fig. 3(d)) showed a strip-shaped distribution and the highest values occurred in Inner Mongolia, indicating that air masses from long-distance transport played a key role during the pre-LCD. During the LCD (Fig. 3(e)), Shandong Province and the Beijing-Tianjin-Hebei (BTH) regions were identified as the high potential source region for amine-containing particles, indicating that amines particles were mainly influenced by surrounding regions during the LCD. In addition, the higher values were distributed over the adjacent sea during the LCD than during the pre-LCD and post-LCD, resulting in the enhanced contribution of sea salt to amine-containing particles as discussed above. As shown in Fig. 3(f), the higher amine WPSCF values were mainly distributed within the most regions of Mongolia, and a few hotspots were also found in Hubei Province during the post-LCD. It implied that long-distance transport played an important role in the amine-containing particle during the post-LCD. Previous study has confirmed that different types of Ca^{2+} can be proposed as the tracers to identify the sources of dust. $CaSO_4$ mainly comes from the local area, but $CaCO_3$ is largely from Chinese dust origin (Yuan et al., 2008). The correlation ($R^2 = 0.62$, $P < 0.01$) between peak area of calcium and sulfate during the LCD was higher than that during the pre-LCD ($R^2 = 0.22$, $P < 0.01$) and post-LCD ($R^2 = 0.28$, $P < 0.01$). In addition, the peak area of calcium was strongly correlated with that of carbonate both during the pre-LCD ($R^2 = 0.72$, $P < 0.01$) and post-LCD ($R^2 = 0.68$, $P < 0.01$), but such a robust correlation was not obtained during the LCD ($R^2 = 0.31$, $P < 0.01$). These results implied that the amine-containing particles were mainly from local and surrounding sources during the LCD, while those were mainly affected by long-range transport during the pre-LCD and post-LCD.

3.5. Impact of the fog events on amine-containing particles

Based on the temporal profiles of amine-containing particles and the amine/total ratio, temperature, RH, and the number count of hydroxymethanesulfonate (HMS) in the detected particles, two fog events were observed during the LCD (marked with gray shadow) and no fog event was obtained in other two observation periods. Here, we took the first fog event from 22:00 on February 7 to 7:00 on February 8 as an example to explore how fog process facilitate the gas-to-particle partitioning of amine particle. The higher average RH (94.1 ± 4.8%) and lower temperature (1.4 ± 0.8 °C) were observed during Fog 1 than those (RH: 63.5 ± 8.5%; T: 8.7 ± 2.4 °C) during clear days. The number of amine-containing particles was significantly enhanced when fog events occurred (Fig. S8), which was also observed in previous studies (Zhang et al., 2012; Zhang and Anastasio, 2003). The ratio of amine/total detected particles during fog events (0.27) was 1.4 times higher than that (0.19) during clear days, indicating that fog events could promotes the formation of amine-containing particles. As a marker of aqueous-phase fog process, the counts of HMS particle also dramatically increased during fog events. It provided evidence that fog events could promote the aqueous formation of amine-containing particles. It is worth noting that the count of amines peaked at 4:00 in the morning when the ambient RH reached up to 96 % during Fog 1 (Fig. S8). Moreover, the fraction of amine-containing particles was closely correlated with RH ($R^2 = 0.74$, $P < 0.01$) and ALWC ($R^2 = 0.70$, $P < 0.01$) during Fog 1, but such strong correlations were not obtained during clear days ($R^2 < 0.45$, $P < 0.01$) and in the whole sampling periods ($R^2 < 0.1$, $P > 0.05$) as discussed in section 3.3. These results suggested that both RH and ALWC played a vital role in the partitioning of gaseous amines into the aerosol phase when fog process was formed. Theoretical calculation have demonstrated that the lower temperature and higher RH conditions facilitated the gas-to-particle partitioning of amine (Hu et al., 2008). Therefore, the count of amine-containing particles was negatively correlated with temperature ($R^2 = 0.48$, $P < 0.01$) during fog events. As shown in Fig. S9, the amine-containing particles mainly distributed in the submicron size of 0.3–1.2 μm during clear days and fog events. The size distribution of amine-containing particles became wider and the counts increased along with the fog formation, indicating that fog processes may have enhanced the gas-to-particle partitioning of amine-containing particles. These results implied that fog events could favor the growth of particles, owing to the enhancement of RH and ALWC, as well as the enhanced gas-to-particle partitioning.

The relative contributions of SO_4^{2-} and NO_3^- to $PM_{2.5}$ during fog events were 15.0 ± 0.9% and 17.4 ± 0.8%, which increased by 1.8 and 1.2 times than those (SO_4^{2-}: 8.2 ± 1.1%; NO_3^-: 14.7 ± 1.7%) during clear days, suggesting that the enhanced production of SO_4^{2-} and NO_3^- through fog processes. In addition, the concentrations of SO_4^{2-} and NO_3^- exhibited strong correlations with RH ($R^2 > 0.82$, $P < 0.01$) and ALWC ($R^2 > 0.66$, $P < 0.01$) during fog events, again confirming that the higher water content during fog process could enhance the production of both two species. The percentage of NH_4^+ during clear days was 15.2 ± 1.7 %, which dropped slightly to 14.8 ± 0.4 % during fog events. The concentrations of NH_4^+ showed a slightly increasing trend from the beginning (7.7 μg m^{-3}) to the end (10.6 μg m^{-3}) of Fog 1. In addition, NH_4^+ exhibited strong correlations with RH and ALWC during fog events ($R^2 > 0.30$, $P < 0.01$), suggesting that the fog process could enhance the production of ammonium. The above discussions confirmed that particulate amines principally existed in the forms of aminium salts such as aminium sulfate and aminium nitrate. To determine the relationships between amine, ammonium, nitrate and sulfate in amine-containing particles during fog events, the temporal variations in the peak areas of amines, ammonium, sulfate and nitrate in amine-containing particles were shown in Fig. 4. The peak area variation of different species detected by the SPAMS is a reliable indicator of the atmospheric process in individual particles (Lian et al., 2020b). As shown in Fig. 4(a), the peak areas of amines, ammonium, nitrate and sulfate had a similar pattern of variations in fog events. The peak area of amines exhibited robustly correlations with peak areas of nitrate and sulfate ($R^2 > 0.94$, $P < 0.01$). However, those correlations became weaker in clear days ($R^2 < 0.61$, $P < 0.01$), suggesting that the fog events could enhance the production of aminium sulfate and aminium nitrate. Moreover, the peak areas of ammonium also showed strong correlations with nitrate ($R^2 = 0.87$, $P < 0.01$) and sulfate ($R^2 = 0.84$, $P < 0.01$) during fog events, but relatively weaker correlations with nitrate ($R^2 = 0.49$, $P < 0.01$) and sulfate ($R^2 = 0.57$, $P < 0.01$) in clear days.

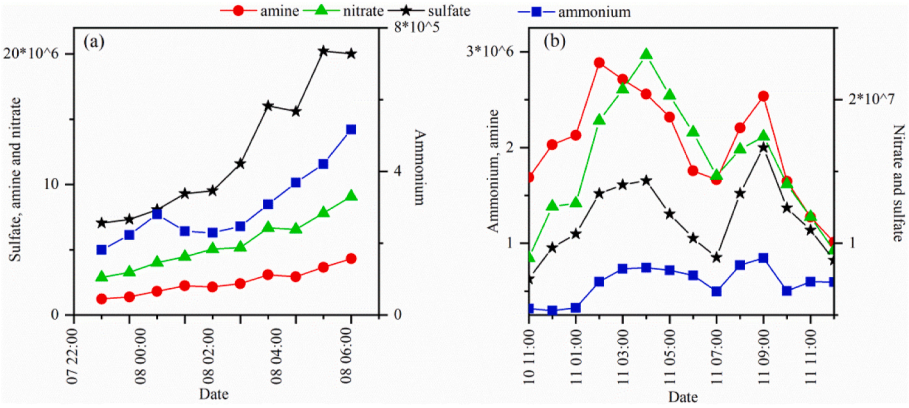

Fig. 4. Temporal variations in the peak areas of amine, ammonium, nitrate and sulfate in amine-containing particles during (**a**) Fog 1, and (**b**) clear days.

Apparently, the higher water content during fog events greatly enhanced the acid-base reaction in amine-containing particles.

4. Summary and conclusions

The substantial drop in on-road vehicular traffic, and manufacturing activities during the LCD resulted in a sharp drop in air pollutants such as $PM_{2.5}$, SO_2, NO_x, and CO. Similarly, the count and relative abundance of amine-containing particles in total detected particles showed a decreasing trend throughout the observation period, which could be attributed to the reduced emission strength of amines and suppressed gas-to-particle partitioning of amines during the LCD and post-LCD. The most abundant particle type was $^{74}(C_2H_5)_2NH_2^+$, accounting for approximately 98 % of all amine-containing particles in the whole observation period, followed by $^{86}[(C_2H_5)_2NCH_2^+$ or $C_3H_7NHC_2H_4^+]$, and $^{59}(CH_3)_3N^+$. R_{ra} during the post-LCD was 80.0 ± 71.8, which was about twice higher than that during the pre-LCD (38.8 ± 21.5) and LCD (33.6 ± 16.1), suggesting that the more acidic nature of amine-containing particles during the post-LCD. The increased aerosol acidity and lower temperature conditions was favorable for the gas-to-particle partitioning of amine-containing particles, while the impacts of RH and ALWC were minor. The broader size peak and distribution range of amine-containing particles during the LCD and post-LCD than during the pre-LCD was possibly resulted from more complex sources and/or gaseous amine condensation or reaction with coarser particles. More than 96 % of amines were found to be mixed with sulfate and nitrate in the whole sampling period, indicating the possible production of aminium sulfate and nitrate salts. The A-OC particles were the most abundant type, contributing to approximately 40 % of the total amine particles in the whole sampling period. The fraction of A-EC particle (1.1 %) during the LCD was about 2.5 times lower than that in the pre-LCD (3.8 %) and post-LCD (3.7 %), owing to the sharp reduction of on-road vehicle numbers in the LCD. The fog events could promote the aqueous formation and growth of amine-containing particles, due primarily to the enhancement of RH and ALWC. In addition, nitrate and sulfate were more strongly associated with amine and ammonium in amine-containing particles during the fog events. The results indicating that higher water content during fog events could enhance the acid-base reaction in amine-containing particles. The results suggested that amines could promote the formation of sulfate and nitrate under the higher RH conditions, which further played an important role in the aging processes of OAs. Our study improves our understanding of the mixing states and potential roles of amine-containing particles during the COVID-19 outbreak, which provides an important theoretical base for better understanding the origin and evolution of OAs in the NCP and joint-control and balanced strategy for air pollution control.

Author contributions

J.M. designed and supervised the whole project. Z.L. and J.M. conducted the experiments and performed the data analyses. Z.L. and J.M. wrote the manuscript. All authors contributed to the paper with useful scientific discussions or comments.

Declaration of competing interest

The authors declare that they have no known competing financial interests or personal relationships that could have appeared to influence the work reported in this paper.

Acknowledgements

This work was supported by the National Science Foundation of China (Grant Nos. 41505112 and 41702373) and the Natural Science Foundation of Shandong Province (Grant No. ZR2020MD113) and the Open Funds of State Key Laboratory of Loess and Quaternary Geology, Institute of Earth Environment, Chinese Academy of Sciences (Grant No. SKLLQG2020).

Appendix A. Supplementary data

Supplementary data to this article can be found online at https://doi.org/10.1016/j.envpol.2021.117887.

References

Almeida, J., Schobesberger, S., Kürten, A., Ortega, I.K., Kupiainen-Määttä, O., Praplan, A. P., Adamov, A., Amorim, A., Bianchi, F., Breitenlechner, M., David, A., Dommen, J., Donahue, N.M., Downard, A., Dunne, E., Duplissy, J., Ehrhart, S., Flagan, R.C., Franchin, A., Guida, R., Hakala, J., Hansel, A., Heinritzi, M., Henschel, H., Jokinen, T., Junninen, H., Kajos, M., Kangasluoma, J., Keskinen, H., Kupc, A., Kurtén, T., Kvashin, A.N., Laaksonen, A., Lehtipalo, K., Leiminger, M., Leppä, J., Loukonen, V., Makhmutov, V., Mathot, S., McGrath, M.J., Nieminen, T., Olenius, T., Onnela, A., Petäjä, T., Riccobono, F., Riipinen, I., Rissanen, M., Rondo, L., Ruuskanen, T., Santos, F.D., Sarnela, N., Schallhart, S., Schnitzhofer, R., Seinfeld, J. H., Simon, M., Sipilä, M., Stozhkov, Y., Stratmann, F., Tomé, A., Tröstl, J., Tsagkogeorgas, G., Vaattovaara, P., Viisanen, Y., Virtanen, A., Vrtala, A., Wagner, P. E., Weingartner, E., Wex, H., Williamson, C., Wimmer, D., Ye, P., Yli-Juuti, T., Carslaw, K.S., Kulmala, M., Curtius, J., Baltensperger, U., Worsnop, D.R., Vehkamäki, H., Kirkby, J., 2013. Molecular understanding of sulphuric acid–amine particle nucleation in the atmosphere. Nature 502, 359–363.

Angelino, S., Suess, D.T., Prather, K.A., 2001. formation of aerosol particles from reactions of secondary and tertiary Alkylamines: characterization by aerosol time-of-flight mass spectrometry. Environ. Sci. Technol. 35, 3130–3138.

Bao, R., Zhang, A.C., 2020. Does lockdown reduce air pollution? Evidence from 44 cities in northern China. Sci. Total Environ. 731.

Bi, X., Zhang, G., Li, L., Wang, X., Li, M., Sheng, G., Fu, J., Zhou, Z., 2011. Mixing state of biomass burning particles by single particle aerosol mass spectrometer in the urban area of PRD, China. Atmos. Environ. 45, 3447–3453.

Bzdek, B.R., Ridge, D.P., Johnston, M.V., 2010. Amine exchange into ammonium bisulfate and ammonium nitrate nuclei. Atmos. Chem. Phys. 10, 3495–3503.

Chang, Y., Huang, R.-J., Ge, X., Huang, X., Hu, J., Duan, Y., Zou, Z., Liu, X., Lehmann, M. F., 2020. Puzzling haze events in China during the coronavirus (COVID-19) shutdown. Geophys. Res. Lett. 47, e2020GL088533.
Chen, Y., Tian, M., Huang, R.J., Shi, G., Wang, H., Peng, C., Cao, J., Wang, Q., Zhang, S., Guo, D., Zhang, L., Yang, F., 2019. Characterization of urban amine-containing particles in southwestern China: seasonal variation, source, and processing. Atmos. Chem. Phys. 19, 3245–3255.
Cheng, C., Huang, Z., Chan, C.K., Chu, Y., Li, M., Zhang, T., Ou, Y., Chen, D., Cheng, P., Li, L., Gao, W., Huang, Z., Huang, B., Fu, Z., Zhou, Z., 2018. Characteristics and mixing state of amine-containing particles at a rural site in the Pearl River Delta, China. Atmos. Chem. Phys. 18, 9147–9159.
Cheng, G., Hu, Y., Sun, M., Chen, Y., Chen, Y., Zong, C., Chen, J., Ge, X., 2020. Characteristics and potential source areas of aliphatic amines in PM2.5 in Yangzhou, China. Atmos. Pollut. Res. 11, 296–302.
Creamean, J.M., Ault, A.P., Ten Hoeve, J.E., Jacobson, M.Z., Roberts, G.C., Prather, K.A., 2011. Measurements of aerosol chemistry during new particle formation events at a remote rural mountain site. Environ. Sci. Technol. 45, 8208–8216.
Dai, Q.L., Bi, X.H., Liu, B.S., Li, L.W., Ding, J., Song, W.B., Bi, S.Y., Schulze, B.C., Song, C. B., Wu, J.H., Zhang, Y.F., Feng, Y.C., Hopke, P.K., 2018. Chemical nature of PM2.5 and PM10 in Xi'an, China: insights into primary emissions and secondary particle formation. Environ. Pollut. 240, 155–166.
Denkenberger, K.A., Moffet, R.C., Holecek, J.C., Rebotier, T.P., Prather, K.A., 2007. Real-time, single-particle measurements of oligomers in aged ambient aerosol particles. Environ. Sci. Technol. 41, 5439–5446.
Ge, X., Wexler, A.S., Clegg, S.L., 2011a. Atmospheric amines – Part I. A review. Atmos. Environ. 45, 524–546.
Ge, X., Wexler, A.S., Clegg, S.L., 2011b. Atmospheric amines – Part II. Thermodynamic properties and gas/particle partitioning. Atmos. Environ. 45, 561–577.
Healy, R.M., Evans, G.J., Murphy, M., Sierau, B., Arndt, J., McGillicuddy, E., O'Connor, I. P., Sodeau, J.R., Wenger, J.C., 2015. Single-particle speciation of alkylamines in ambient aerosol at five European sites. Anal. Bioanal. Chem. 407, 5899–5909.
Hu, M., Wu, Z., Slanina, J., Lin, P., Liu, S., Zeng, L., 2008. Acidic gases, ammonia and water-soluble ions in PM2.5 at a coastal site in the Pearl River Delta, China. Atmos. Environ. 42, 6310–6320.
Huang, X., Ding, A.J., Gao, J., Zheng, B., Zhou, D.R., Qi, X.M., Tang, R., Wang, J.P., Ren, C.H., Nie, W., Chi, X.G., Xu, Z., Chen, L.D., Li, Y.Y., Che, F., Pang, N.N., Wang, H.K., Tong, D., Qin, W., Cheng, W., Liu, W.J., Fu, Q.Y., Liu, B.X., Chai, F.H., Davis, S.J., Zhang, Q., He, K.B., 2021. Enhanced secondary pollution offset reduction of primary emissions during COVID-19 lockdown in China. Natl. Sci. Rev. 8.
Huang, Y., Chen, H., Wang, L., Yang, X., Chen, J., 2012. Single particle analysis of amines in ambient aerosol in Shanghai. Environ. Chem. 9, 202.
Jia, H., Huo, J., Fu, Q., Duan, Y., Lin, Y., Jin, X., Hu, X., Cheng, J., 2020. Insights into chemical composition, abatement mechanisms and regional transport of atmospheric pollutants in the Yangtze River Delta region, China during the COVID-19 outbreak control period. Environ. Pollut. 267, 115612.
Kirkby, J., Curtius, J., Almeida, J., Dunne, E., Duplissy, J., Ehrhart, S., Franchin, A., Gagné, S., Ickes, L., Kürten, A., Kupc, A., Metzger, A., Riccobono, F., Rondo, L., Schobesberger, S., Tsagkogeorgas, G., Wimmer, D., Amorim, A., Bianchi, F., Breitenlechner, M., David, A., Dommen, J., Downard, A., Ehn, M., Flagan, R.C., Haider, S., Hansel, A., Hauser, D., Jud, W., Junninen, H., Kreissl, F., Kvashin, A., Laaksonen, A., Lehtipalo, K., Lima, J., Lovejoy, E.R., Makhmutov, V., Mathot, S., Mikkilä, J., Minginette, P., Mogo, S., Nieminen, T., Onnela, A., Pereira, P., Petäjä, T., Schnitzhofer, R., Seinfeld, J.H., Sipilä, M., Stozhkov, Y., Stratmann, F., Tomé, A., Vanhanen, J., Viisanen, Y., Vrtala, A., Wagner, P.E., Walther, H., Weingartner, E., Wex, H., Winkler, P.M., Carslaw, K.S., Worsnop, D.R., Baltensperger, U., Kulmala, M., 2011. Role of sulphuric acid, ammonia and galactic cosmic rays in atmospheric aerosol nucleation. Nature 476, 429–433.
Kurten, A., Bergen, A., Heinritzi, M., Leiminger, M., Lorenz, V., Piel, F., Simon, M., Sitals, R., Wagner, A.C., Curtius, J., 2016. Observation of new particle formation and measurement of sulfuric acid, ammonia, amines and highly oxidized organic molecules at a rural site in central Germany. Atmos. Chem. Phys. 16, 12793–12813.
Le, T., Wang, Y., Liu, L., Yang, J., Yung, Y.L., Li, G., Seinfeld, J.H., 2020. Unexpected air pollution with marked emission reductions during the COVID-19 outbreak in China. Science, eabb7431.
Lee, D., Wexler, A.S., 2013. Atmospheric amines – Part III: photochemistry and toxicity. Atmos. Environ. 71, 95–103.
Li, L., Huang, Z., Dong, J., Li, M., Gao, W., Nian, H., Fu, Z., Zhang, G., Bi, X., Cheng, P., Zhou, Z., 2011. Real time bipolar time-of-flight mass spectrometer for analyzing single aerosol particles. Int. J. Mass Spectrom. 303, 118–124.
Li, L., Li, Q., Huang, L., Wang, Q., Zhu, A., Xu, J., Liu, Z., Li, H., Shi, L., Li, R., Azari, M., Wang, Y., Zhang, X., Liu, Z., Zhu, Y., Zhang, K., Xue, S., Ooi, M.C.G., Zhang, D., Chan, A., 2020a. Air quality changes during the COVID-19 lockdown over the Yangtze River Delta Region: an insight into the impact of human activity pattern changes on air pollution variation. Sci. Total Environ. 732, 139282.
Li, Z., Meng, J., Zhou, L., Zhou, R., Fu, M., Wang, Y., Yi, Y., Song, A., Guo, Q., Hou, Z., Yan, L., 2020b. Impact of the COVID-19 event on the characteristics of atmospheric single particle in the northern China. Aerosol Air Qual. Res. 20, 1716–1726.
Lian, X., Huang, J., Huang, R., Liu, C., Wang, L., Zhang, T., 2020a. Impact of city lockdown on the air quality of COVID-19-hit of Wuhan city. Sci. Total Environ. 742, 140556.
Lian, X., Zhang, G., Lin, Q., Liu, F., Peng, L., Yang, Y., Fu, Y., Jiang, F., Bi, X., Chen, D., Wang, X., Peng, P.a., Sheng, G., 2020b. Seasonal variation of amine-containing particles in urban Guangzhou, China. Atmos. Environ. 222, 117102.
Liu, F., Bi, X., Zhang, G., Lian, X., Fu, Y., Yang, Y., Lin, Q., Jiang, F., Wang, X., Peng, P.a., Sheng, G., 2018. Gas-to-particle partitioning of atmospheric amines observed at a mountain site in southern China. Atmos. Environ. 195, 1–11.
Liu, F.X., Bi, X.H., Zhang, G.H., Peng, L., Lian, X.F., Lu, H.Y., Fu, Y.Z., Wang, X.M., Peng, P.A., Sheng, G.Y., 2017. Concentration, size distribution and dry deposition of amines in atmospheric particles of urban Guangzhou, China. Atmos. Environ. 171, 279–288.
Liu, L., Zhang, J., Du, R.G., Teng, X.M., Hu, R., Yuan, Q., Tang, S.S., Ren, C.H., Huang, X., Xu, L., Zhang, Y.X., Zhang, X.Y., Song, C.B., Liu, B.W., Lu, G., Shi, Z.B., Li, W.J., 2021. Chemistry of atmospheric fine particles during the COVID-19 pandemic in a megacity of eastern China. Geophys. Res. Lett. 48.
Lloyd, J.A., Heaton, K.J., Johnston, M.V., 2009. Reactive uptake of trimethylamine into ammonium nitrate particles. J. Phys. Chem. 113, 4840–4843.
Meng, J.J., Li, Z., Zhou, R.W., Chen, M., Li, Y.Y., Yi, Y.N., Ding, Z.J., Li, H.J., Yan, L., Hou, Z.F., Wang, G.H., 2021. Enhanced photochemical formation of secondary organic aerosols during the COVID-19 lockdown in Northern China. Sci. Total Environ. 758.
Monks, P.S., Archibald, A.T., Colette, A., Cooper, O., Coyle, M., Derwent, R., Fowler, D., Granier, C., Law, K.S., Mills, G.E., Stevenson, D.S., Tarasova, O., Thouret, V., von Schneidemesser, E., Sommariva, R., Wild, O., Williams, M.L., 2015. Tropospheric ozone and its precursors from the urban to the global scale from air quality to short-lived climate forcer. Atmos. Chem. Phys. 15, 8889–8973.
Murphy, S.M., Sorooshian, A., Kroll, J.H., Ng, N.L., Chhabra, P., Tong, C., Surratt, J.D., Knipping, E., Flagan, R.C., Seinfeld, J.H., 2007. Secondary aerosol formation from atmospheric reactions of aliphatic amines. Atmos. Chem. Phys. 7, 2313–2337.
Pei, Z., Han, G., Ma, X., Su, H., Gong, W., 2020. Response of major air pollutants to COVID-19 lockdowns in China. Sci. Total Environ. 743, 140879.
Qin, X., Pratt, K.A., Shields, L.G., Toner, S.M., Prather, K.A., 2012. Seasonal comparisons of single-particle chemical mixing state in Riverside, CA. Atmos. Environ. 59, 587–596.
Rehbein, P., Jeong, C.-H., McGuire, M., Yao, X., Corbin, J., Evans, G., 2011. Cloud and fog processing enhanced gas-to-particle partitioning of trimethylamine. Environ. Sci. Technol. 45, 4346–4352.
Sauerwein, M., Chan, C.K., 2017. Heterogeneous uptake of ammonia and dimethylamine into sulfuric and oxalic acid particles. Atmos. Chem. Phys. Discuss. 17, 1–28.
Shen, W.C., Ren, L.L., Zhao, Y., Zhou, L.Y., Dai, L., Ge, X.L., Kong, S.F., Yan, Q., Xu, H.H., Jiang, Y.J., He, J., Chen, M.D., Yu, H.A., 2017. C1-C2 alkyl aminiums in urban aerosols: insights from ambient and fuel combustion emission measurements in the Yangtze River Delta region of China. Environ. Pollut. 230, 12–21.
Sorooshian, A., Murphy, S.M., Hersey, S., Gates, H., Padro, L.T., Nenes, A., Brechtel, F.J., Jonsson, H., Flagan, R.C., Seinfeld, J.H., 2008. Comprehensive airborne characterization of aerosol from a major bovine source. Atmos. Chem. Phys. 8, 5489–5520.
Sun, Y.L., Lei, L., Zhou, W., Chen, C., He, Y., Sun, J.X., Li, Z.J., Xu, W.Q., Wang, Q.Q., Ji, D.S., Fu, P.Q., Wang, Z.F., Worsnop, D.R., 2020. A chemical cocktail during the COVID-19 outbreak in Beijing, China: insights from six-year aerosol particle composition measurements during the Chinese New Year holiday. Sci. Total Environ. 742.
Tang, X.C., Price, D., Praske, E., Lee, S.A., Shattuck, M.A., Purvis-Roberts, K., Silva, P.J., Asa-Awuku, A., Cocker, D.R., 2013. NO3 radical, OH radical and O-3-initiated secondary aerosol formation from aliphatic amines. Atmos. Environ. 72, 105–112.
Tobías, A., Carnerero, C., Reche, C., Massagué, J., Via, M., Minguillón, M.C., Alastuey, A., Querol, X., 2020. Changes in air quality during the lockdown in Barcelona (Spain) one month into the SARS-CoV-2 epidemic. Sci. Total Environ. 726, 138540.
Wang, P., Chen, K., Zhu, S., Wang, P., Zhang, H., 2020. Severe air pollution events not avoided by reduced anthropogenic activities during COVID-19 outbreak. Resour. Conserv. Recycl. 158, 104814.
Wang, Y.Q., Zhang, X.Y., Draxler, R.R., 2009. TrajStat: GIS-based software that uses various trajectory statistical analysis methods to identify potential sources from long-term air pollution measurement data. Environ. Model. Software 24, 938–939.
Wu, Z.J., Wang, Y., Tan, T.Y., Zhu, Y.S., Li, M.R., Shang, D.J., Wang, H.C., Lu, K.D., Guo, S., Zeng, L.M., Zhang, Y.H., 2018. Aerosol liquid water driven by anthropogenic inorganic salts: implying its key role in haze formation over the North China plain. Environ. Sci. Technol. Lett. 5, 160–166.
Xu, J.Z., Ge, X.L., Zhang, X.H., Zhao, W.H., Zhang, R.X., Zhang, Y.Z., 2020a. COVID-19 impact on the concentration and composition of submicron particulate matter in a typical city of northwest China. Geophys. Res. Lett. 47.
Xu, K., Cui, K., Young, L.-H., Hsieh, Y.-K., Wang, Y.-F., Zhang, J., Wan, S., 2020b. Impact of the COVID-19 event on air quality in Central China. Aerosol Air Qual. Res. 20, 915–929.
Xu, W., Liu, X.J., Liu, L., Dore, A.O., Tang, A.H., Lu, L., Wu, Q.H., Zhang, Y.Y., Hao, T.X., Pan, Y.P., Chen, J.M., Zhang, F.S., 2019. Impact of emission controls on air quality in Beijing during APEC 2014: implications from water-soluble ions and carbonaceous aerosol in PM2.5 and their precursors. Atmos. Environ. 210, 241–252.
Yao, L., Garmash, O., Bianchi, F., Zheng, J., Yan, C., Kontkanen, J., Junninen, H., Mazon, S.B., Ehn, M., Paasonen, P., Sipila, M., Wang, M.Y., Wang, X.K., Xiao, S., Chen, H.F., Lu, Y.Q., Zhang, B.W., Wang, D.F., Fu, Q.Y., Geng, F.H., Li, L., Wang, H. L., Qiao, L.P., Yang, X., Chen, J.M., Kerminen, V.M., Petaja, T., Worsnop, D.R., Kulmala, M., Wang, L., 2018. Atmospheric new particle formation from sulfuric acid and amines in a Chinese megacity. Science 361, 278.
Yi, Y., Meng, J., Hou, Z., Wang, G., Zhou, R., Li, Z., Li, Y., Chen, M., Liu, X., Li, H., Yan, L., 2021. Contrasting compositions and sources of organic aerosol markers in summertime PM2.5 from urban and mountainous regions in the North China Plain. Sci. Total Environ. 766, 144187.
Yuan, H., Zhuang, G.S., Li, J., Wang, Z.F., Li, J., 2008. Mixing of mineral with pollution aerosols in dust season in Beijing: revealed by source apportionment study. Atmos. Environ. 42, 2141–2157.
Yuan, Q., Qi, B., Hu, D.Y., Wang, J.J., Zhang, J., Yang, H.Q., Zhang, S.S., Liu, L., Xu, L., Li, W.J., 2021. Spatiotemporal variations and reduction of air pollutants during the

COVID-19 pandemic in a megacity of Yangtze River Delta in China. Sci. Total Environ. 751.
Zhang, G., Bi, X., Chan, L.Y., Li, L., Wang, X., Feng, J., Sheng, G., Fu, J., Li, M., Zhou, Z., 2012. Enhanced trimethylamine-containing particles during fog events detected by single particle aerosol mass spectrometry in urban Guangzhou, China. Atmos. Environ. 55, 121–126.
Zhang, J., Yuan, Q., Liu, L., Wang, Y., Zhang, Y., Xu, L., Pang, Y., Zhu, Y., Niu, H., Shao, L., Yang, S., Liu, H., Pan, X., Shi, Z., Hu, M., Fu, P., Li, W., 2021. Trans-Regional transport of haze particles from the North China plain to Yangtze River Delta during winter. J. Geophys. Res. Atmos. 126, e2020JD033778.
Zhang, Q., Anastasio, C., 2003. Free and combined amino compounds in atmospheric fine particles (PM2.5) and fog waters from Northern California. Atmos. Environ. 37, 2247–2258.
Zheng, H., Kong, S., Chen, N., Yan, Y., Liu, D., Zhu, B., Xu, K., Cao, W., Ding, Q., Lan, B., Zhang, Z., Zheng, M., Fan, Z., Cheng, Y., Zheng, S., Yao, L., Bai, Y., Zhao, T., Qi, S., 2020. Significant changes in the chemical compositions and sources of PM2.5 in Wuhan since the city lockdown as COVID-19. Sci. Total Environ. 739, 140000.